Lab on a Chip

Accepted Manuscript

ROYAL SOCIETY OF CHEMISTRY

www.rsc.org/loc

Lab on a Chip

RSCPublishing

COMMUNICATION

Integrated optofluidic device for single-cell sorting driven by mechanical properties

Cite this: DOI: 10.1039/x0xx00000x

T. Yang,[a†] P. Paiè,[b,c†] G. Nava,[a] F. Bragheri,[c] R.Martinez Vazquez,[c] P. Minzioni,[a*] M. Veglione,[d] M. Di Tano,[d] C. Mondello,[d] R. Osellame[b,c] and I. Cristiani[a]

Received 00th January 2012,
Accepted 00th January 2012

DOI: 10.1039/x0xx00000x

www.rsc.org/

We present a novel optofluidic device for real-time sorting on the basis of cell mechanical properties, measured by optical stretching. The whole mechanism, based on optical forces, does not hamper the viability of the tested cells, which can be used for further analysis. The device effectiveness is demonstrated by extracting a sample population enriched in highly metastatic cells out of a heterogeneous cell mixture.

It is widely reported in the literature that mechanical properties are an intrinsic and reliable marker of cell status and can be used to distinguish specific cells out of a heterogeneous population[1–3]. At the present state of the art, the optical stretching technique is recognized as an efficient and contactless tool to probe the mechanical properties at the single cell level. Several papers have already demonstrated that cell optical deformability allows distinguishing healthy, tumorigenic and metastatic cells, and that it can be used to study the effects of different drugs treatment on cell mechanical response[4–6]. Here we report the design, fabrication and test of a novel integrated microfluidic optical device, which is capable of performing single cell stretching and recovery according to cells' measured optical deformability. The chip is based on a double-Y-shaped microfluidic circuit in which cells flow in a laminar regime. Both stretching and subsequent sorting are realized by optical forces, exerted through the laser radiation emitted from optical waveguides which are integrated in the chip substrate and perfectly aligned to the microfluidic channel. The outcome of the stretching procedure provides information on the mechanical properties of each measured cell, which can be used to decide whether to sort the cell or not.

[a] *Dipartimento di Ingegneria Industriale e dell'Informazione, Università di Pavia, Via Ferrata 5A, 27100 Pavia, Italy. Email: paolo.minzioni@unipv.it; Tel: +39 0382 98522; Fax: +39 0382 422583*
[b] *Dipartimento di Fisica, Politecnico di Milano,Piazza Leonardo da Vinci 32, 20133 Milano, Italy*
[c] *Istituto di Fotonica e Nanotecnologie (IFN)-CNR,Piazza Leonardo da Vinci 32, 20133 Milano, Italy*
[d] *Istituto di Genetica Molecolare (IGM)-CNR, Via Abbiategrasso 207, 27100 Pavia, Italy*
† These authors contributed equally to the work
†† Electronic supplementary information (ESI) available.

To this aim, cell deformability must be quantified by a real-time evaluation of the cell shape, thus requiring a high quality imaging for the trapped and stretched cell inside the microchannel. This microfluidic chip is fabricated in a small glass volume (1.1×3.5×2 mm) by femtosecond laser irradiation followed by chemical etching (FLICE), similarly to what is already reported in the literature[7–12]. The main limitation that hinders a good cell imaging for stretching measurement is internal channel wall roughness[9,13,14], which can be greatly reduced by properly optimizing the irradiation geometry. As shown in[15], if the channel is written transversely with respect to the writing laser beam direction (Fig. 1(a)), the roughness is lower at the sidewalls than at the channel top and bottom. Since the latter surfaces are the ones through which we image the stretched cells (see green arrow in Fig. 1(a)), we introduced a different writing geometry to improve the quality of the relevant surfaces. In particular, we fabricate the microfluidic channels parallel to the writing beam by irradiating them from the bottom to the top of the substrate, as schematically shown in Fig. 1(b). The central channel, with a square cross-section, is obtained by irradiating overlapped squares at different depths. Laser polarization is always kept parallel to the writing direction.

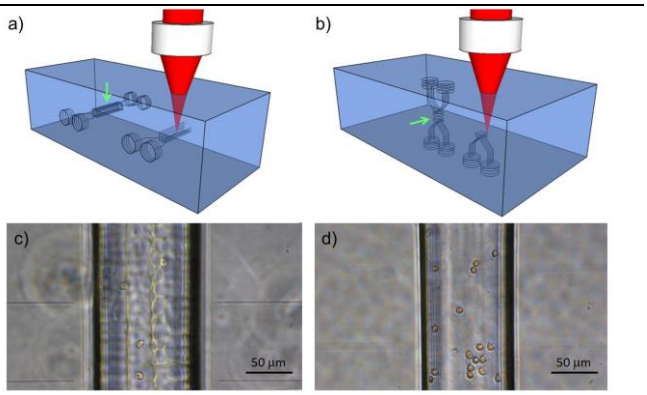

Fig. 1 Schematic rendering of the double-Y-shaped microfluidic circuit irradiation patterns and phase-contrast microscope images of swollen red blood cells in microchannels fabricated with the two geometries: (a), (c) transverse and (b), (d) longitudinal writing geometry.

Fig. 1(c) and 1(d) display two phase-contrast microscope images (taken along the direction indicated by the green arrow in Fig. 1a and 1b) of swollen red blood cells in microchannels fabricated with the two geometries. The images demonstrate a significant improvement in the microchannel surface quality with this new approach.

The reason for the surface quality improvement in lateral surfaces with respect to bottom surfaces still needs further investigation. It has been suggested that this is due to a more favorable alignment of the nanogratings induced in the irradiation process[15], although this is not consistent with the results of our optimization process. Our opinion is that the main reason is related to the highly ellipsoidal shape of the writing voxel. The lateral surfaces are indeed produced by the longer dimension of the voxel, while the top/bottom ones are created by the sharper part. For a given separation of the irradiated tracks, a much larger overlap and better uniformity is therefore expected in the former case.

The detailed fabrication process is described in the following. The first step consists in laser irradiation by focusing the second harmonic pulses of a commercial femtosecond laser source (femtoREGEN, HighQlaser) through a 50×, 0.6 NA microscope objective. The laser power and scanning velocity are varied along the substrate depth to overcome the effects of spherical aberrations: the irradiation is performed with an energy of 400 nJ and a translation speed of 0.07 mm/s for the bottom Y-branch, 300 nJ and 0.1 mm/s for the central square channel, 300 nJ and 0.2 mm/s for the top Y-branch. To produce the central square channel we irradiated a pattern of 60 μm squares at different depths (with a separation of 2 μm over a total length of 300 μm). Vertical lines are also irradiated inside the squares to facilitate glass removal by the acid. The Y-shaped branches are obtained by multiscan irradiation of 10 lines in order to obtain, after etching, channel with the same height as the central one. Access holes for the tubing connection are realized by irradiating 4 coaxial circular helixes at each termination of the Y-branches. The irradiation pattern is shown in Fig. 1(b). After irradiation, the glass substrate is immersed in a 20% aqueous solution of hydrofluoric acid at 35°C in an ultrasonic bath for 1.5 hours. In the same irradiation step we also fabricate the optical waveguides for the stretching and sorting functionalities by using pulses of 60 nJ energy and a scan speed of 0.01 mm/s. Single mode waveguides at 1070 nm, with a mode diameter of 8 μm and measured propagation losses of about 3 dB/cm are thus obtained. End faces are finally polished to allow fiber pigtailing to the optical waveguides.

The chip is then connected to a computer-controlled system shown in Fig. 2, including a 10 W Ytterbium fiber laser (emission wavelength 1070 nm), two micropumps, an electrically actuated translator and a phase-contrast microscope. The optical fiber from the laser is spliced to a 50/50 coupler, in order to split the optical power evenly in two single mode fibers, and each of them is jointed to a fiber-to-fiber U-bench and then pigtailed to the optical waveguide integrated inside the chip. The chip is mounted on an inverted microscope equipped with a 40× objective and connected to a CCD camera. Two vials are filled respectively with the cell suspension and a buffer solution (PBS, or culture medium), and the vials' content is injected into the two inlets of the microchip at a precisely controlled flow rate determined by the micropumps. Thanks to the laminar regime of the flow, all cells injected at the input port 1 are recovered at the port 3 that corresponds to the waste. In the stretching and sorting procedure, the following steps are performed.

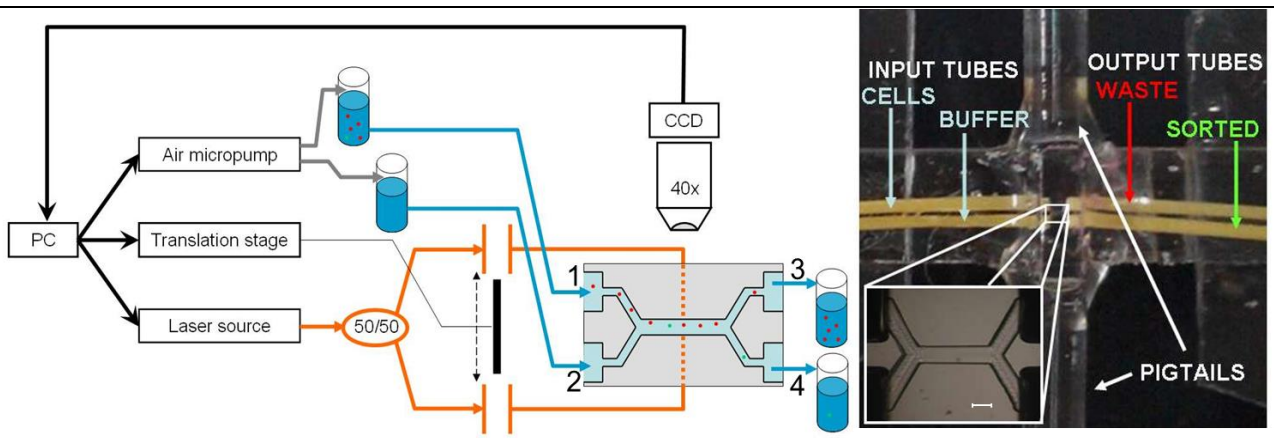

Fig. 2 Left: schematic representation of the experimental setup used to validate our novel optofluidic microchip. Cell stretching and sorting are based on the optical forces exerted by the same waveguides, which are connected with fiber-to-fiber U-bench to realize the automatic sorting. Right: picture of the optofluidic chip connected to external capillaries and fiber pigtails. The locally enlarged image shows the inside structure of the microchannel network (Scale bar, 100 μm).

Laser emission is first turned on and the cell is trapped by the radiation emitted by each waveguide (about 5 mW). The laser power is then raised (maximum power per side 1.2 W) for 5s and the selected cell is stretched. During cell stretching, the computer continuously captures and analyzes the CCD image to evaluate the cell deformation in real-time. The optically induced stretching, characterized as a change of cell ellipticity, is extracted through a standard edge-detection algorithm including a correction factor for the applied optical forces that takes into account the initial cell dimensions[6] (additional data and figures are reported in the supplementary material). According to the measured maximum deformation and a selected threshold, the cell is then redirected to one of the two output channels. To smoothly address the cell to the selected output, the computer automatically moves a beam blocker to one or the other of the two U-benches, creating an unbalanced radiation pressure on the cell, and thus moving it towards a precise output. The whole scheme is shown in Fig. 2 along with a picture of optofluidic chip.

This system has been experimentally tested by performing stretching and sorting experiments with a cell mixture containing the same concentration of metastatic (A375P) and highly-metastatic (A375MC2) human melanoma cells16. It is worth underlining that A375MC2 and A375P cells were simply chosen as a device-validation test, given their different optical deformability, correlated to the different metastatic potential.

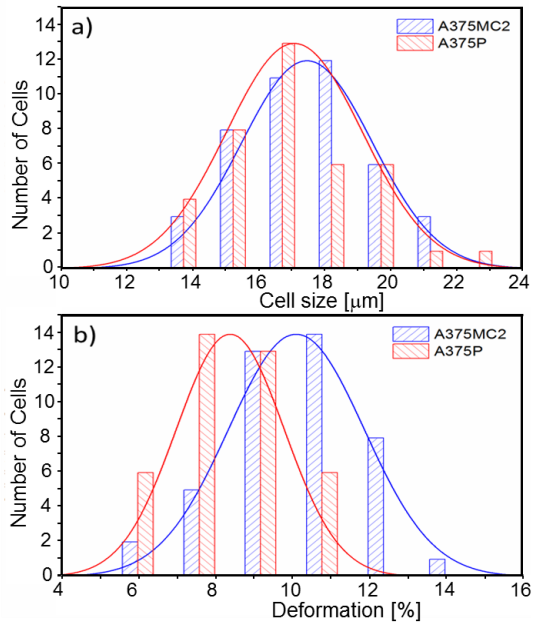

Fig. 3 Characterization of the (a) cellular size and (b) deformability of the two cell lines A375MC2 and A375P. They show a very similar cellular diameter, 17 ± 2 μm, but a different deformability: 8.4 ± 1.1 % for A375P and 10.1± 1.8 % for A375MC2 when the laser output power is 1.2 W.

Nevertheless, in the current reported experiment the ability to separate cells with high deformability can lead to the study of drugs that affects the mechanical properties of metastatic cells, as well as to a deeper comprehension of genetic factors related to cell metastatic abilities.The two cell lines are characterized by a very similar cellular diameter (17 ± 2 μm), as confirmed by the experimental results shown in Fig. 3(a); it is therefore impossible to distinguish the two cell lines, when they are not labelled. Nonetheless, as reported in Fig. 3(b) a different deformability is found when they are analysed with the optical stretcher; hence mechanical cell properties can be used as a marker to separate them. In particular when the laser output power is 1.2 W per fibre, a deformation of 8.4 ± 1.1 % for A375P and 10.1± 1.8 % for A375MC2 is shown; these values are obtained by fitting the experimental data with a Gaussian curve, after verifying the normality of the two distributions. From these experimental results, the theoretical deformation distribution of A375MC2 and A375P is reported by the two colour lines in Fig. 4(a). These curves are calculated from the experimental deformability measurements, by normalizing these values so that the integral area of the curves are equal, since in the sample cells are mixed under 1:1 ratio. As a consequence, a sample with an increased concentration of highly metastatic (A375MC2) cells can be obtained by selecting those cells whose deformability is above a certain threshold. It is evident that by increasing the threshold value the percentage of highly deformable cells in the sample will increase. However, it is worth underlining that choosing a higher threshold implies that a lower percentage of cells will exhibit deformability higher than the threshold. This percentage of cell, which can be defined as the "acceptance rate" of the sorting measurement, can be easily calculated and is shown as dashed line in Fig. 4(b). According to the normalized cell distribution over its optical deformability in Fig. 4(a), the theoretical values of A375MC2 enrichment ratio are also calculated and plotted in Fig. 4(b) as continuous line. When the threshold is very low, almost all of A375MC2 and A375P cells are collected. Therefore A375MC2 percentage in the collected sample is almost the same as in the starting mixture (50%). By increasing the threshold the more deformable cells are selectively sorted resulting in an increased percentage of highly metastatic cells in the sample collected at output 4. To experimentally validate the system, four different deformation thresholds were considered: 8, 9, 10 and 11%, and for each value the measurement was repeated 5 times, collecting every time a number of cells between 60 and 80. To distinguish the two cell lines within the collected cells, A375MC2 cells were previously stained with a fluorescent dye (LDS 751).

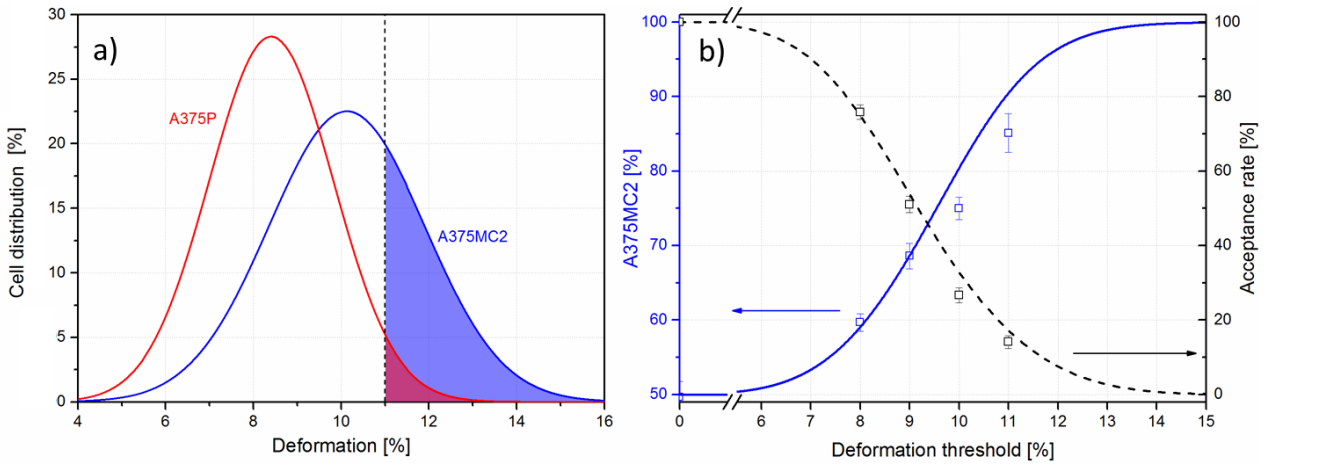

Fig. 4 a) A375 and A375MC2 normalized cellular distribution as a function of their optical deformation. The whole area under each cell curve is set equal because the two cell lines are mixed with the same concentration. By choosing a specific value of deformation as threshold, an enriched A375MC2 subpopulation is obtained by collecting cells with deformability higher than the threshold. As an example, we represented a 11% threshold and the coloured areas shows the number of cells expected in the collected sample for this threshold deformation value. b) Percentage of A375MC2 in the sorted cells output and of cells in the initial sample that are expected to exhibit a deformability higher than the threshold (acceptance rate) as a function of deformation threshold. Experimental points are reported together with the theoretical curves. Error bars are standard deviations.

The percentage of highly metastatic cells in the suspension, obtained by counting the number of fluorescent cells in the sample collected at the output port 4 under each experimental setting, is then compared with theoretical results expected by the deformability distribution of the two cell lines shown in Fig. 4. As an example in Fig. 4(a), we chose to highlight a 11% threshold. Hence the coloured areas represent the amount of cells that will be sorted. As clearly visible a small overlap between the two curves is still present, hence we expect to have cells of both lines in the collected sample. Anyway, such threshold value leads to the prediction of a 90% of highly metastatic cells within the collected sample. From the experiment we obtained a value of 85%; which is in good agreement with the theoretical predictions. Moreover, by considering the experimental values obtained for all the tested threshold, the results, as shown in Fig. 4(b), demonstrate the effectiveness of the device, showing that the percentage of A375MC2 cells in the sorted cell sample closely matches the theoretical one when the threshold is relatively low, and only a small deviation from the theoretical curve is observed when the deformation threshold is increased (5% for the highest value). The reduction of device performance observed by increasing the threshold can be explained considering that a higher threshold implies a lower cell acceptance rate as previously discussed. Consequently, achieving the same number of sorted cells requires longer measurement duration, thus favouring the formation of cells clusters, which can affect the flow laminarity and hence the proper functioning of the microchip.

It's worth noticing that in order to achieve high deformations, high laser powers are usually exploited, which may damage the measured cells. To test this possible drawback, we analysed cellular viability after the sorting and stretching procedure. Using two different methods, Trypan blue staining and *in vitro* cultures of sorted cells, we demonstrated that cellular viability and proliferation are not altered by the cell passage through the chip and subsequent stretching (see Supplementary information). The percentage of dead cells in the sorted sample was in the range 2-6% and it was comparable to that for reference samples, whose cells were not stretched. Moreover the viability results are also in good agreement with the data reported in literature[5,17]: irradiating the cells for 5s at a laser power of 1.2W per fibre, yields a 20°C increase in cell temperature. Since during the experiments the chip is kept at 20°C, cells are subjected to a moderate temperature (~40°C) for a short time, a condition that is not expected to cause thermal damages or a heat shock response[17,18].

Conclusions

The proposed device enables an effective stretching, sorting and collection of single cells on the basis of their mechanical properties. Its effectiveness has been demonstrated by extracting a sub-population of highly deformable cells starting from a mixture of human melanoma cells with different metastatic potential. An increase from 50% to 85% in the A375MC2 concentration is demonstrated, with a 1.7 enrichment factor closely matching the theoretically expected one. This value, however, greatly depends on the samples under study and could be largely enhanced if samples with a smaller overlap in the deformability distributions have to be analysed. This novel device can open up a completely new set of biological investigations, ranging from the sorting, separation and analysis of cells with different mechanical properties within a population of "nominally identical cells", to the selection and recovery of cells showing specific mechanical response to drug treatments, thus offering new opportunities in many different research fields. In particular, given the device characteristics (single cell analysis, high purity of collected sample, low throughput) it appears as a good candidate for the selection of rare single cells as, for example, tumour stem cells. Sorted cells could then be subjected to further analysis allowing the identification of genetic and cellular markers linked to specific biological processes.

Acknowledgements

The authors thank Dr. Richard Hynes (Howard Hughes Medical Institute, Center for Cancer Research, MIT) for the generous gift of A375 and A375MC2 cells. Financial support is also acknowledged to Fondazione Cariplo through the grant ''Optofluidic chips for the study of cancer cell mechanical properties and invasive capacities'' (Ref. # 2011-0370) and to Progetto Bandiera "La Fabbrica del Futuro" in the framework of the funded project PLUS.

Notes and references

1. W. Zhang, K. Kai, D. S. Choi, T. Iwamoto, Y. H. Nguyen, H. Wong, M. D. Landis, N. T. Ueno, J. Chang, L. Qin, *Proc. Natl. Acad. Sci.*, 2012, **109**, 18707–18712.
2. A. E. Ekpenyong, G. Whyte, K. Chalut, S. Pagliara, F. Lautenschläger, C. Fiddler, S. Paschke, U. F. Keyser, E. R. Chilvers, J. Guck, *PLoS One*, 2012, **7**, e45237.
3. Q. Guo, S. Park, and H. Ma, *Lab Chip*, 2012, **12**, 2687–2695.
4. F. Lautenschläger, S. Paschke, S. Schinkinger, A. Bruel, M. Beil, and J. Guck, *Proc. Natl. Acad. Sci.*, 2009, **106**, 15696–15701.
5. J. Guck, R. Ananthakrishnan, H. Mahmood, T. J. Moon, C. C. Cunningham, and J. Käs, *Biophys. J.*, 2001, **81**, 767–784.
6. J. Guck, S. Schinkinger, B. Lincoln, F. Wottawah, S. Ebert, M. Romeyke, D. Lenz, H. M. Erickson, R. Ananthakrishnan, D. Mitchell, J. Käs, S. Ulvick, and C. Bilby, *Biophys. J.*, 2005, **88**, 3689–3698.
7. R. R. Gattass and E. Mazur, *Nat Phot.*, 2008, **2**, 219–225.
8. B.-B. Xu, Y.-L. Zhang, H. Xia, W.-F. Dong, H. Ding, and H.-B. Sun, *Lab Chip*, 2013, **13**, 1677–90.
9. F. Bragheri, P. Minzioni, R. Martinez Vazquez, N. Bellini, P. Paie, C. Mondello, R. Ramponi, I. Cristiani, R. Osellame, *Lab Chip*, 2012, **12**, 3779–3784.
10. R. Osellame, V. Maselli, R. M. Vazquez, R. Ramponi, G. Cerullo, *Appl. Phys. Lett.*, 2007, **90**, 231113–231118.
11. K. Sugioka, J. Xu, D. Wu, Y. Hanada, Z. Wang, Y. Cheng, K. Midorikawa, *Lab Chip*, 2014, **14**, 3447–58.
12. D. Choudhury, W. T. Ramsay, R. Kiss, N. A. Willoughby, L. Paterson, A. K. Kar, *Lab Chip*, 2012, **12**, 948–53.
13. F. Bragheri, L. Ferrara, N. Bellini, K. C. Vishnubhatla, P. Minzioni, R. Ramponi, R. Osellame, I. Cristiani, *J. Biophotonics*, 2010, **3**, 234–243.
14. N. Bellini, K. C. Vishnubhatla, F. Bragheri, L. Ferrara, P. Minzioni, R. Ramponi, I. Cristiani, R. Osellame, *Opt. Express*, 2010, **18**, 4679–4688.
15. S. Ho, P. R. Herman, J. S. Aitchison, *Appl. Phys. A*, 2011, **106**, 5–13.
16. L. Xu, S. Begum, J. D. Hearn, R. O. Hynes, *Proc. Natl. Acad. Sci. U. S. A.*, 2006, **103**, 9023–8.
17. F. Wetzel, S. Rönicke, K. Müller, M. Gyger, D. Rose, M. Zink, J. Käs, *Eur. Biophys. J.*, 2011, **40**, 1109–14.
18. V. Ortner, A. Ludwig, E. Riegel, S. Dunzinger, T. Czerny, *Cell Stress and Chaperones*, 2014, 1-12.